Requirements for the assimilation of cloudy radiances

F. Chevallier, P. Bauer, G. Kelly, J.-F. Mahfouf, C. Jakob, T. McNally

European Centre for Medium-Range Weather Forecasts

Summary: Radiation observations such as those from the Advanced Tiros Operational Vertical Sounder on-board the National Oceanic and Atmospheric Administration satellites provide information about cloud systems. However, like the other cloud observations they are not used in global data assimilation systems.

In the first part of this paper, cloudy radiances are used to evaluate the characteristics of the cloud fields produced by the European Centre for Medium-Range Weather Forecasts forecasting system over mid-latitude and tropical oceans during two seasons of the 40-year re-analysis that is currently being produced. Observed and model-generated radiances, as well as derived cloud parameters, are compared. The model dynamics is shown to distribute the clouds well, with realistic seasonal cycles. However, deficiencies are identified and discussed: the cloud radiative impact in the mid-latitudes appears to be too low, the frequency of occurrence of high clouds is overestimated in the inter-tropical convergence zone and the stratocumulus off the West coast of the continents is underestimated. The methods described here provide a framework for assessing the impact of improvements to the cloud scheme.

In the second part of the paper, prospects for the use of cloudy radiances in a data assimilation system are considered using a one-dimensional variational analysis (1D-Var) scheme. In non-rainy areas, it is shown that the 1D-Var can remove, create and modify the cloud variables to fit the observed radiances. The benefit of such information is discussed with a single-column model. Having a consistent analysis of clouds and dynamics appears to be the key advantage of the variational framework for the assimilation of cloud information.

1 Introduction

Numerical Weather Prediction (NWP) models require accurate initial conditions and therefore rely heavily on the quality of the assimilation schemes. Pressure, temperature, water vapour, and wind information from conventional and satellite observations have been operationally assimilated at global NWP centres for a long time. Despite the major influence of clouds on the atmosphere water and energy balance, there is still no explicit cloud analysis in global systems. At the European Centre for Medium-Range Weather Forecasts (ECMWF), more than half of the satellite radiances is not used by the global analysis system because it is suspected of being impacted by clouds. Studies have shown that these cloudy areas may correspond to regions where key analysis errors are located, and therefore are crucial for the quality of the forecasts (McNally 2000).

The main reason why global analysis systems do not include cloud information is that cloud processes contain small spatial and temporal scales not explicitly described by NWP models. Observing and modelling cloud 4D variability is difficult. However, even though surface precipitation has similar features, positive impact of assimilation of Tropical Rainfall Measuring Mission (TRMM) -derived surface rainfall rates has been observed (Marécal and Mahfouf 2000). These authors use a one-dimensional variational (1D-Var) scheme to extract the model-resolved-scale information on temperature and moisture from the surface rainfall rates. In this paper, observations from the TIROS-N Operational Vertical Sounder (TOVS) instruments on-board the National Oceanic and Atmospheric Administration (NOAA) satellites are used to study similar prospects for cloud assimilation.

The TOVS data are first used to assess the characteristics of the cloud fields produced by the ECMWF forecast system. 6-hour forecasts from a test production of the 40-year (from 1957 onward) re-analysis that has been undertaken recently (ERA-40: Simmons and Gibson 2000) are compared to the High-

resolution Infrared Radiation Sounder/2 (HIRS/2) and Microwave Sounding Unit (MSU) data from the TOVS over mid-latitude and tropical oceans (60°S-60°N). The data and the model are described in section 2. Use is made both of the radiances themselves and of HIRS/2-derived cloud variables using the CO_2-slicing technique described by Wylie *et al.* (1994). Model-equivalent infrared and micro-wave radiances are computed from the model variables using a forward radiation scheme detailed in section 3. The MSU radiance comparison is presented in section 4. The HIRS radiance and the HIRS-derived cloud variable comparisons are shown in section 5. The results are discussed in section 6.

The assimilation of cloud information is expected to help correcting some identified model deficiencies. In order to evaluate these prospects, the Advanced TOVS (ATOVS) data are used in a 1D-Var scheme. The impact of this assimilation is studied in a single-column model through sensitivity studies to initial conditions. The results are presented and discussed in section 7.

2 The data

2.1 The TOVS data

The MSU radiometer of TOVS comprises four channels for making passive measurements in the 5.5 millimetre wavelength oxygen region. Their weighting functions respectively peak at the surface, at 700hPa, at 300hPa and at 90hPa. An MSU spot has a typical circular shape of 54.7 *km* radius at nadir and an elliptic shape of axis 323.1 and 178.8 *km* at the end of the scan (Kidwell 1998).

The HIRS/2 instrument of TOVS measures radiation in 20 channels covering both the long-wave and the short-wave parts of the spectrum. The ground instantaneous field of view is typically a circle of 17.4 km diameter at nadir. At the end of the scan, the ground field of view is 58.5 km cross-track by 29.9 km along-track (Kidwell 1998).

Satellite	NOAA-09	NOAA-10
launch	Dec. 1984	Sep. 1986
ascending node	1420	1930

Table 1: Launch date and approximate time of the ascending node (northbound Equator crossing) in Local Solar Time (LST) for NOAA-09 and NOAA-10 when the satellites were launched. Due to the satellite's orbits drift over time, the Equator crossing time for NOAA-09 is close to 1500 LST for the period studied (Price 1991).

The raw radiances for HIRS and MSU are taken here from the NOAA-09 and NOAA-10 satellites. Both of them operate in a near-polar, sun-synchronous orbit, with about 14 orbits per day. As reported in table 1, they cross the Equator at different times and therefore provide some information about the diurnal cycle of the Earth-atmosphere system when combined together. Due to the high volume of data, only one HIRS spot over four is processed here, irrespective of scan angle. All MSU spots are used.

Various biases affect the brightness temperatures throughout the life of an instrument. The data used here are bias-corrected with the ECMWF operational method described by Harris and Kelly (2001). The computed biases can reach several kelvins in some channels. In the framework of the CO_2-slicing method described below, these corrections were shown to improve the consistency between the different channels.

2.2 The model fields

The model data come from a test run of the ECMWF 40-year re-analysis. The forthcoming final version of the re-analysis will differ only by minor improvements from the system used in the present test run.

The assimilation system relies on the 3-dimensional variational scheme described by Courtier *et al.*, Rabier *et al.* and Andersson *et al.* (1998). It includes the TOVS raw radiances that are diagnosed as not affected by clouds. Also, with impact on the hydrological cycle, radiosonde and surface data, cloud-wind product from geostationary satellites, scatterometer winds, column water vapour and surface winds from Special Sensor Microwave Imager (SSM/I, from August 1987) are assimilated. Analyses are performed at 00, 06, 12 and 18 UTC.

The forecast model is a global spectral $T_L159L60$ model. It includes a semi-Lagrangian advection scheme together with a linear Gaussian grid (Hortal 1999). The reduced horizontal grid corresponds to a regular grid size of about 125 *km* from the equator to the poles. In the vertical, a hybrid coordinate of 60 levels between the surface and the top of the atmosphere is used by the global spectral forecast model. The physics package is an improved version of that described by Gregory *et al.* (2000). In particular, the prognostic cloud scheme is a revised version of that defined by Tiedtke (1993), with details of the revisions described in Jakob (1994), Jakob and Klein (2000), Jakob (2000) and Jakob *et al.* (2000). The broad-band radiation scheme includes the Rapid Radiative Transfer Model (Mlawer *et al.*, 1997) for the infrared and the Fouquart and Bonnel (1980) scheme (with four spectral bands) for the short-wave. The surface scheme is based on the new tiled treatment described by Van den Hurk *et al.* (2000).

In the following, 6-hour forecasts at 00, 06, 12 and 18 UTC are compared to the TOVS data in the 6-hour window that is centred around the forecast time. Model data are interpolated at observation points and at observation times. As the resolution of the observations and that of the model differ, emphasis is put here on seasonal statistics rather than on instantaneous comparisons. Both boreal winter 1986-1987 (DJF) and summer 1987 (JJA) are considered.

3 Comparing model and satellite data

3.1 Clear-sky radiative transfer

For a stratified cloudless atmosphere in local thermodynamical equilibrium, the top-of-the-atmosphere up-welling radiance at frequency ν can be written:

$$\begin{aligned} L_\nu^{Clr}(\theta) &= \epsilon_\nu(\theta)\tau_\nu^{\uparrow}(P_0,\theta)B_\nu(T_{P_0}) \\ &\quad +[1-\epsilon_\nu(\theta)]\tau_\nu^{\uparrow}(P_0,\theta)\int_{P_t}^{P_0} B_\nu(T_{P'})\frac{\partial\tau_\nu^{\downarrow}(P',\theta)}{\partial P'}dP' \\ &\quad +\int_{P_0}^{P_t} B_\nu(T_{P'})\frac{\partial\tau_\nu^{\uparrow}(P',\theta)}{\partial P'}dP' \end{aligned} \tag{1}$$

where θ is the zenith angle, $B_\nu(T_P)$ is the Planck function at temperature T_P at pressure level P (with P_0 the surface pressure and P_t the top-of-the-atmosphere pressure), $\tau_\nu^{\uparrow}(P,\theta)$ is the monochromatic transmittance for isotropic radiation between level of pressure P and space, $\tau_\nu^{\downarrow}(P,\theta)$ is the monochromatic transmittance for isotropic radiation between level of pressure P and surface, $\epsilon_\nu(\theta)$ is the surface emissivity. Specular reflection at the surface $(1-\epsilon_\nu(\theta))$ is assumed.

Equation (1) is solved by the Radiative Transfer for Tiros Operational Vertical Sounder (RTTOV:

Eyre, 1991; Saunders *et al.*, 1999) scheme for the computation of clear-sky model-equivalent satellite radiances. RTTOV also handles instruments such as Advanced TOVS (ATOVS) or SSM/I.

3.2 Parameterisation of cloud absorption

In the present study RTTOV is modified so that it takes cloud absorption into account in a way similar to the ECMWF operational broad-band infrared radiation scheme (Morcrette 1991b). Similar work was done for HIRS/2 on a previous version of the ECMWF system but was never used routinely (Rizzi 1994).

Following the multi-layer grey body approach (Washington and Williamson 1977), clouds are introduced as grey bodies. Their contribution to the radiances is determined by their horizontal coverage n^i and their emissivity ϵ_ν^i in each vertical layer i of the model. ϵ_ν^i is derived from the cloud liquid (and/or ice) water path l^i by the following equation:

$$\epsilon_\nu^i = 1 - e^{-k_\nu^i l^i} \tag{2}$$

where k_ν^i is the extinction coefficient at frequency ν. Its value varies according to the nature (liquid or ice) of the cloud, the assumed particle size spectra and particle temperature.

This approach enables the radiances in the presence of semi-transparent cloud layers to be expressed as a linear combination of the clear sky radiance L_ν^{Clr}, and of the radiances in the presence of single layered clouds treated as black bodies, L_ν^i. The coefficients of the linear combination are functions of the n^is and of the ϵ_ν^is and depend on the way the cloudy layers overlap. Surface reflection of the cloud downward emission is taken into account because it has a strong impact over sea for micro-waves.

Various overlapping hypotheses can be used according to the vertical structure of the clouds (Morcrette and Jakob 2000). The maximum-random hypothesis, as described by Räisänen (1998) is used here. It explicitly distinguishes between the horizontal coverage and the emissivity of the cloud layers, as is done in the current operational broad-band scheme.

Cloud absorption is taken into account in the infrared spectrum following Ebert and Curry (1992) for ice water and Smith and Shi (1992) for liquid water. Scattering is usually small for the wavelengths studied here (above 5 μm) at the top of the atmosphere and is therefore neglected. Consistently with the broadband radiation model, ice particle radii vary between 30 and 60 μm with a temperature dependency from Ou and Liou (1995). Liquid particle radius is set to 10 μm over land and 13 μm over sea.

Cloud absorption is introduced in the micro-wave spectrum in the range from 1-200 GHz by a direct function of frequency and liquid water/ice content following Hufford (1991) for ice and Liebe *et al.* (1989) for liquid water. Comparison to Mie-calculations and explicit particle size distributions has shown that scattering by droplets can be neglected for all currently used micro-wave channels while scattering by ice particles may become significant for $\nu > 60$ GHz. The choice of permittivity model may be critical for liquid water at temperatures below 260 K. Rain emission and scattering are not taken into account.

3.3 Strategy for the MSU comparison

Estimating the micro-wave land surface emissivity is difficult (Prigent *et al.* 1997). Over open sea, the lower values of the emissivities (around 0.5) as well as their smaller horizontal variability makes the extraction of information from the micro-wave data easier. As a consequence, the present study

with MSU is restricted to ocean data between 60°S and 60°N only. The Ulaby *et al.* (1981) model provides the sea emissivity.

Among the four MSU channels, the three atmosphere-sounding ones (channels 2 to 4) are not significantly affected by clouds (except channel 2 for deep water clouds). Indeed ice water has negligible impact on the radiances around 50 GHz. Therefore results are presented here for the window channel (channel 1) as the difference between the cloud-affected radiance (either from the model or from the observation) and the clear-sky radiance from the model. In the case of a perfect model, this difference is a function of liquid water and rain profiles only. In fact, uncertainties in the surface temperature and the water vapour profile degrade the accuracy of the model clear-sky radiances. But the largest signal is due to clouds.

3.4 Strategy for the HIRS comparison

Understanding radiance variations in 19 channels is an evolving study. Moreover, the useful information from HIRS is contained not only in the channel brightness temperatures themselves, but also in their relative values with respect to each other.

Among the 20 channels, the present study makes use of four of them (channels 4 to 7) that are located in the CO_2 band around $14\mu m$, and of one (channel 8) that is located in the $11\mu m$ so-called "window" region. First, a similar study to that for MSU is performed on HIRS-8. Then, following the work of Smith and Platt (1978), the CO_2-slicing method is used to retrieve cloud variables from these five channels. The retrieved quantities are the cloud top pressure P_i and the effective cloud amount $(n\epsilon)_\nu$ defined as:

$$L_\nu(\theta) = (n\epsilon)_\nu L^i_\nu(\theta) + [1 - (n\epsilon)_\nu] L^{Clr}_\nu(\theta) \tag{3}$$

where L^i_ν is the top-of-the-atmosphere up-welling radiance emitted at frequency ν by a black-body placed at pressure level P_i.

Assuming that $(n\epsilon)_\nu$ is the same for two adjacent frequencies, equation (3) allows for successive estimations of P_i and of $(n\epsilon)_\nu$. L^i_ν and L^{Clr}_ν are computed here from a previous run of RTTOV from model temperature, absorbing gas profiles and surface characteristics. Four pairs of channels are used from channels 4 to 7 of HIRS. The final variables are those that satisfy the radiative transfer the best. $(n\epsilon)_\nu$ is provided for the 11 μm HIRS channel. As described in Wylie *et al.* (1994), a series of quality checks are performed. If the solution is rejected, a rough estimation is performed using equation (3) with $(n\epsilon)_\nu = 1.0$ in the 11 μm window channel. Retrieved cloud layers below 700 hPa (about 3 km) are most likely to correspond to this simple estimation because the CO_2-slicing method is not capable of retrieving $(n\epsilon)_\nu$ in the lower troposphere.

The sources of error of the method are discussed in Menzel *et al.* (1992). Over open seas, the main issue appears to be multi-layer cloud situations where the algorithm can only retrieve a single layer that may be below the highest transmissive cloud, depending on the emissivity of the clouds below. Due to reduced sensitivity of the infrared sounder in the lower troposphere, as well as to possible temperature inversions close to the surface, the method is not accurate for low clouds.

The CO_2-slicing technique is applied after a rough cloud detection test based on a threshold on channel 8: a cloud is diagnosed when the observed radiance in the 11 μm channel is lower than the model clear sky radiance in the same channel by more than 1 $mW.m^{-2}.sr^{-1}.cm^{-1}$. This cloud detection strongly relies on the quality of the surface temperature estimation. As a consequence, the present study with HIRS is also restricted to ocean data between 60°S and 60°N only, because sea-surface temperature is estimated very accurately from infrared and visible channels observations. It has also a much weaker diurnal cycle than land surface temperature. The sea surface temperature fields come

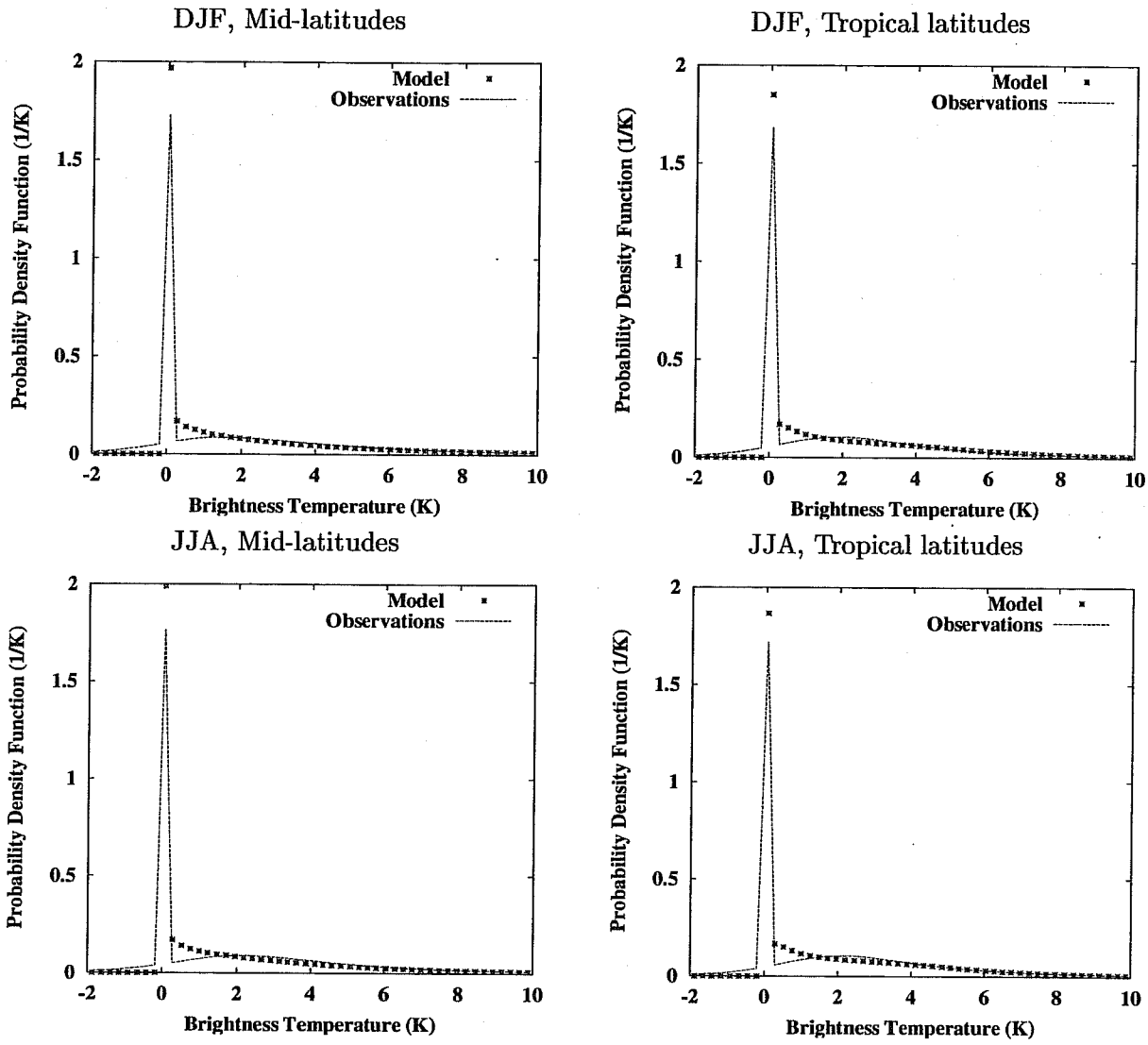

Figure 1: Histograms of the difference between MSU-1 full-sky brightness temperature, either from the model or from the observation, and the model clear sky MSU-1 brightness temperature (i.e. the difference between $(Tb^{Full}_{Obs.} - Tb^{Clr}_{Model})$ and $(Tb^{Full}_{Obs.} - Tb^{Clr}_{Model})$).

from 5-day averages of updated National Center for Environmental Prediction (NCEP) analyses. A functional fit to the tables provided by Masuda *et al.* (1988) provides the infrared sea emissivity (T. J. Kleespies, personal communication).

4 MSU comparison

Figure 1 shows the histograms of the difference between the cloud-affected MSU-1 brightness temperature and the model clear-sky MSU-1 brightness temperature. Distinction is made between boreal winter (DJF) and summer (JJA) seasons, as well as between tropical latitudes (30°N-30°S) and mid-latitudes (60°S-30°S and 30°N-60°N). In all cases, the histograms have the same shape. Around 0 K difference, about 800,000 profiles are not, or nearly not, affected by hydro-meteors. The other bins have much smaller numbers, about 20,000. For the model, the differences are always positive because clouds are seen as warm bodies over the low-emitting sea surface. For the observations, a few profiles

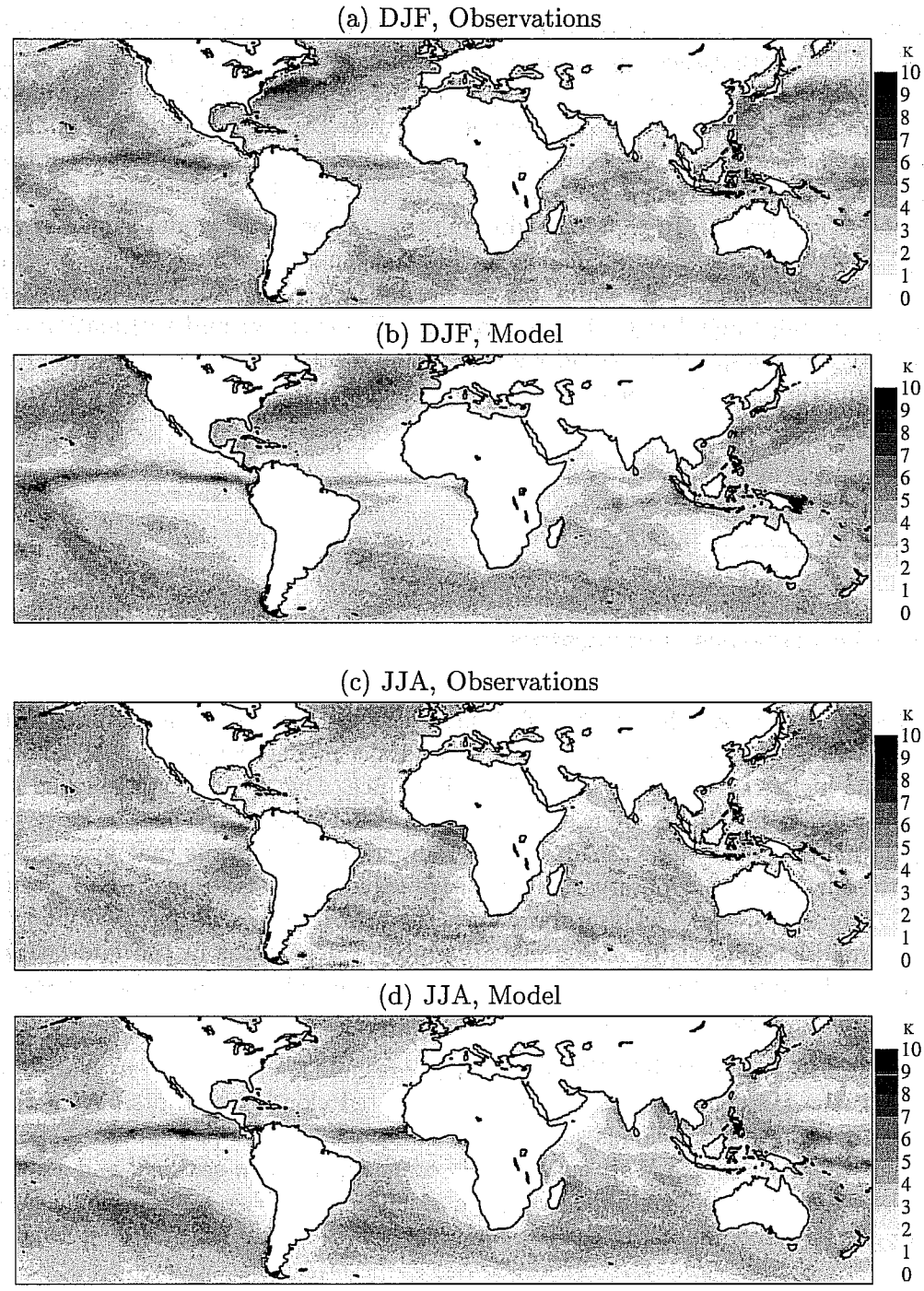

Figure 2: Observed and simulated MSU channel 1 minus model clear-sky MSU channel 1 in the boreal winter (DJF) and summer (JJA) seasons.

show negative values due to inaccurate sea surface temperature and emissivity. The good agreement between the shape of the histograms for the observations and for the model shows the general reliability of these model parameters. Moreover it indicates that the model has a correct proportion of cloud-affected profiles in each latitude band, as seen from the micro-wave radiometer, even though the model slightly overestimates the number of cloud-free cases. It is not possible to draw any quantitative conclusion from the shape of the positive tail, because rain absorption and scattering are not represented in the simulated radiances.

The mean value of the difference between the cloud-affected MSU-1 brightness temperature and the model clear-sky MSU-1 brightness temperature is presented in figure 2 for the two seasons. Few grid points (near the continents) have mean values less than 1 K, which shows that the large amount of small instantaneous values in Figure 1 are spread over much larger regions. Despite the limitations due to impact of rain in the observations, a good qualitative agreement is found in the shape of the ascending-motion regions, like the Inter-Tropical Convergence Zone (ITCZ), the South-Pacific Convergence Zone (SPCZ) and the storm tracks. In the descending-motion regions, the model values are significantly lower than the observation ones. In particular, in the stratocumulus regions off the West coast of the continents, the simulated micro-wave radiances are hardly affected by clouds. This may indicate that the model underestimates liquid water in these regions. However, an underestimation of the surface temperature and/or emissivity there would yield the same result. The study of the infrared radiances brings more information about this matter.

5 HIRS/2 comparison

5.1 HIRS 11μm brightness temperature

Similarly to the MSU-1 study, figures 3 and 4 show the histograms of the difference between the cloud-affected HIRS 11μm brightness temperature and the model clear-sky HIRS 11μm brightness temperature. The histograms peak at about 0 K difference. Due to the high infrared surface emissivity, clouds usually reduce the radiances and therefore the histograms have a large negative tail. Positive values in the model differences are due to temperature inversions that may make the clouds warmer than the surface. In the observations, positive values may also come from inaccurate surface temperature and/or emissivity. The histograms have more variability with latitude than in the micro-wave: the large mid-latitude disturbances make more cold departures in the mid-latitudes than in the tropical band. It appears that the model has less large negative values, that correspond to high clouds, than the observations, in particular in the mid-latitude regions.

As detailed in section 3.4, a cloud detection based on a threshold test on the 11μm channel is used here. Figure 5 presents the frequencies of occurrence of estimated cloud-free points. With this diagnosis, the model appears to have more clouds than the observations in most regions of the globe, except in the stratocumulus regions off the West coast of the continent in both seasons, and around Northern Africa in the boreal summer season only. A lack of cloudiness in these regions is consistent with the micro-wave results presented in section 4. The differences in the other regions are discussed in section 6.

5.2 Retrieved cloud-top pressure

The histograms of cloud-top pressures retrieved by the CO_2-slicing algorithm are presented in Figure 6. The tropical histograms are strongly influenced by the ITCZ, with cloud-top pressures between 200 and 400 hPa as seen from space. A good agreement is found between the model and the observations. In the mid-latitudes, the cloud-top pressures vary much more. Consistently with the HIRS 11μm histogram, the model appears to not correctly represent the highest radiatively-active cloud tops. Also, in both latitude bands, the model has more low clouds than the observations.

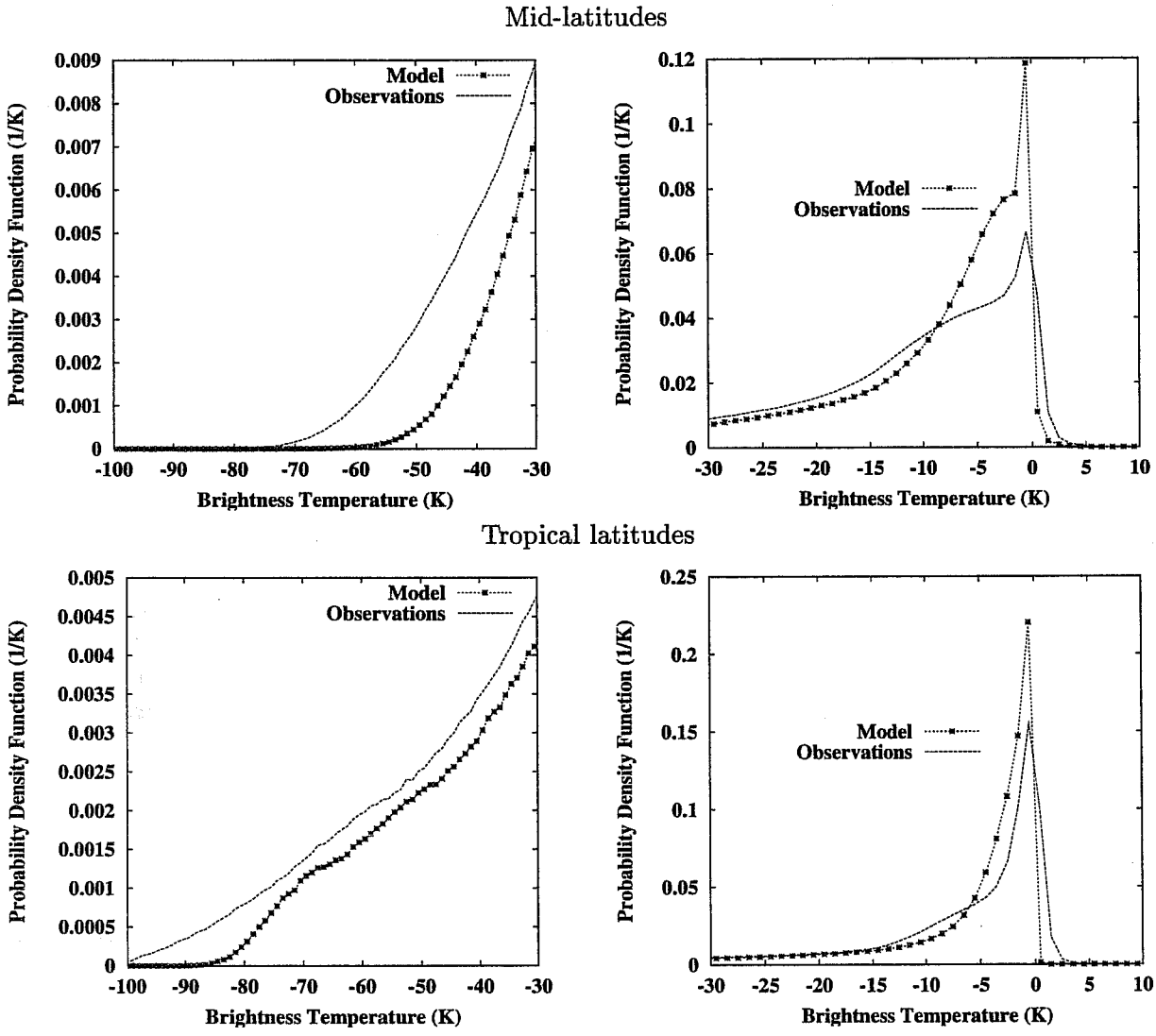

Figure 3: Histograms of the difference between HIRS-08 full-sky brightness temperature, either from the model or from the observation, and the model clear sky HIRS-08 brightness temperature (i.e. the difference between $(Tb_{Obs.}^{Full} - Tb_{Model}^{Clr})$ and $(Tb_{Obs.}^{Full} - Tb_{Model}^{Clr})$). Due to different variation scales, the histograms are divided into two pieces. Boreal winter (DJF) over oceans.

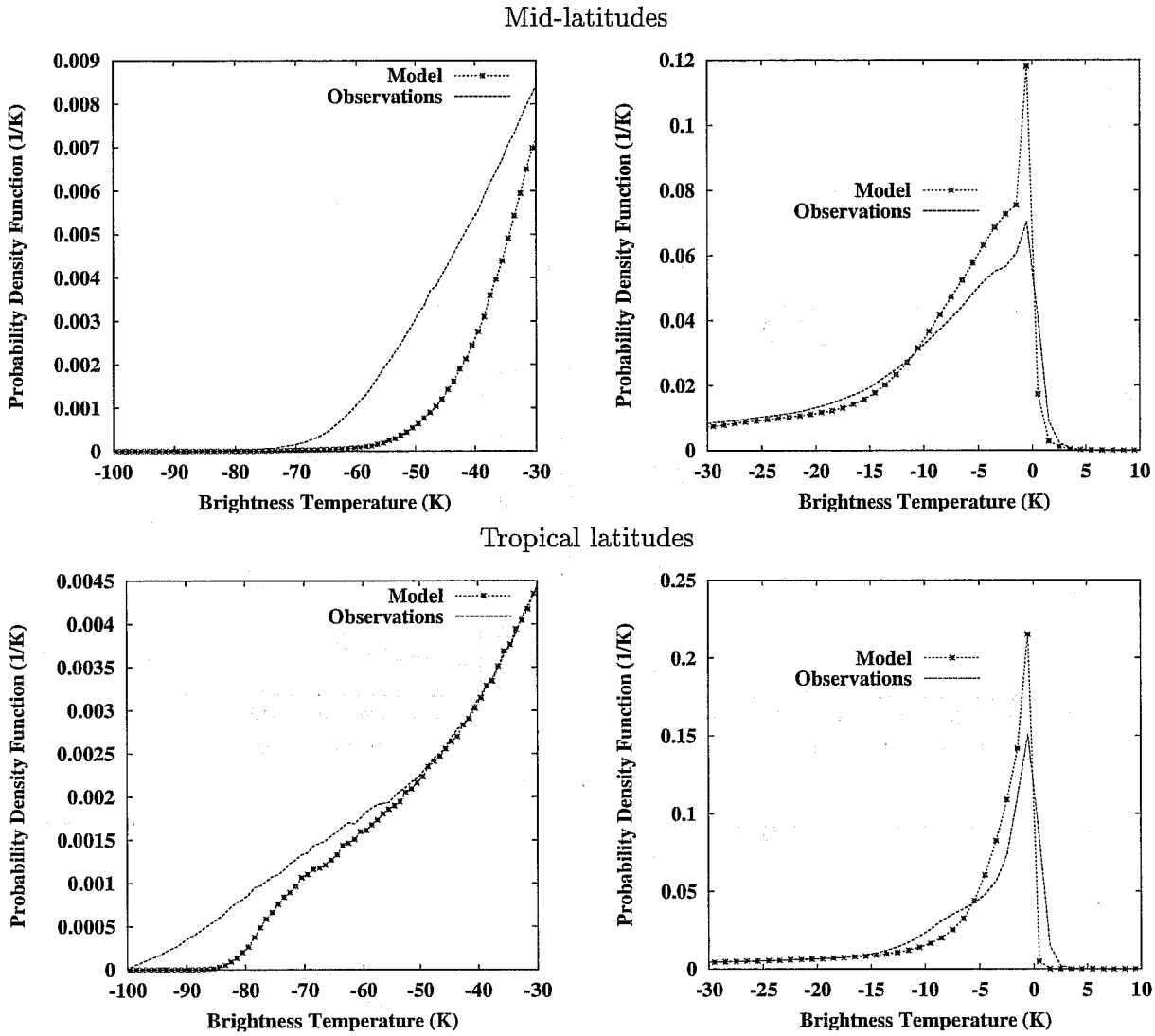

Figure 4: Same as previous, but for the boreal summer (JJA) over oceans.

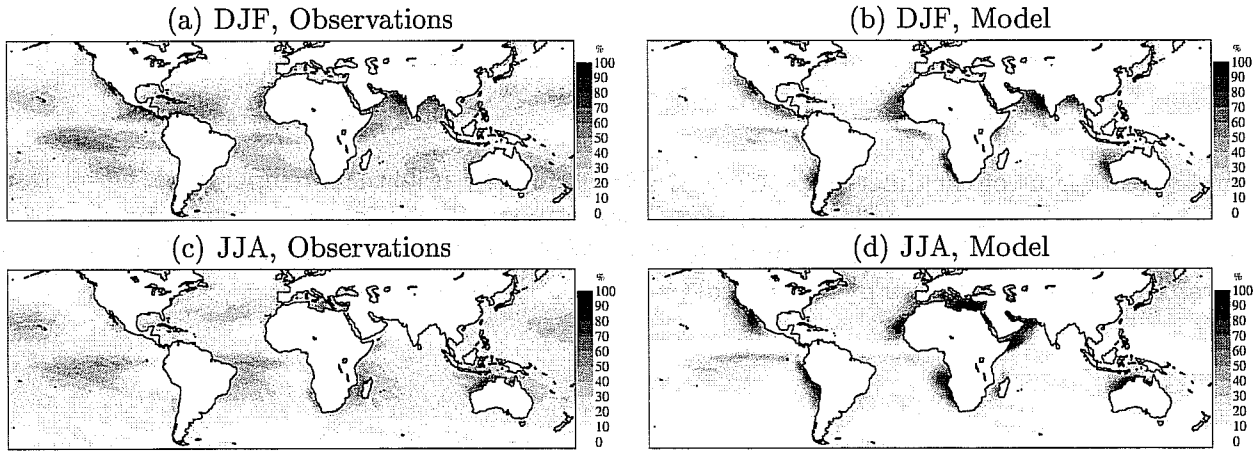

Figure 5: Frequency of clear sky for the boreal winter season (DJF) and the boreal summer season (JJA) over the oceans in the observations (left column) and in the model (right column).

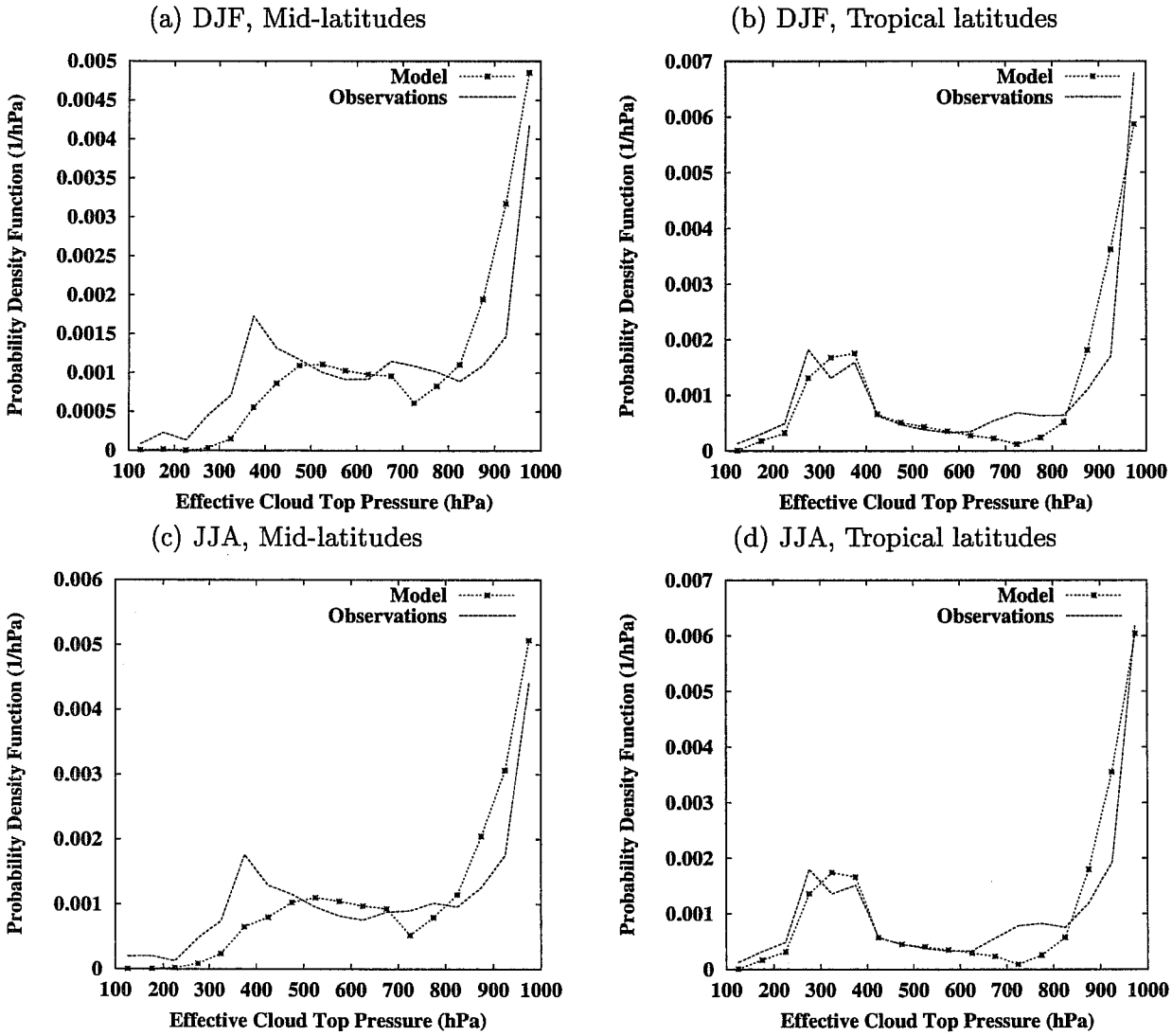

Figure 6: Histograms of effective cloud-top pressure retrieved by the CO_2-slicing method.

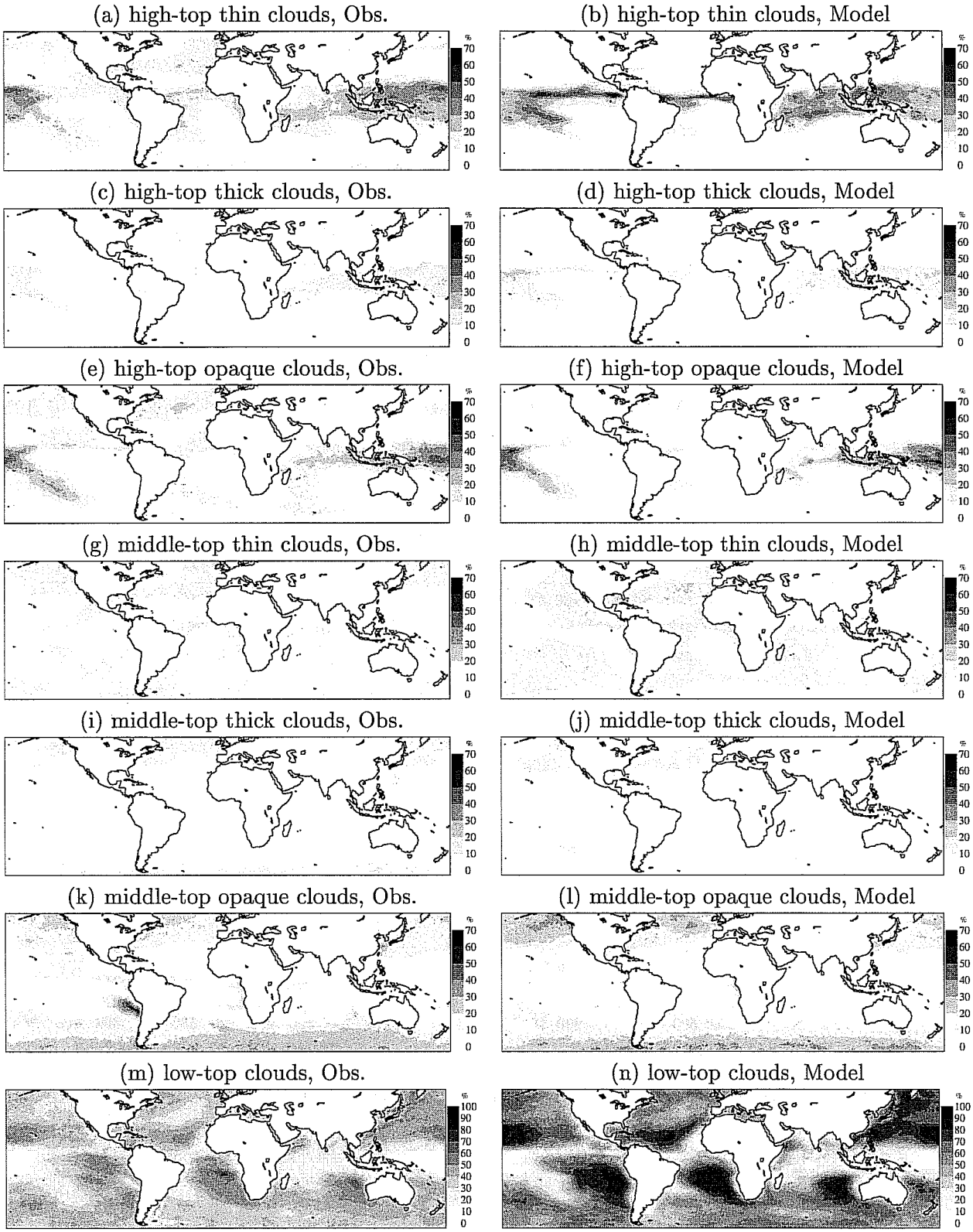

Figure 7: Occurrence frequency of high-, middle- and low-top clouds for the boreal winter season (DJF) over the oceans in the observations (left column) and in the model (right column).

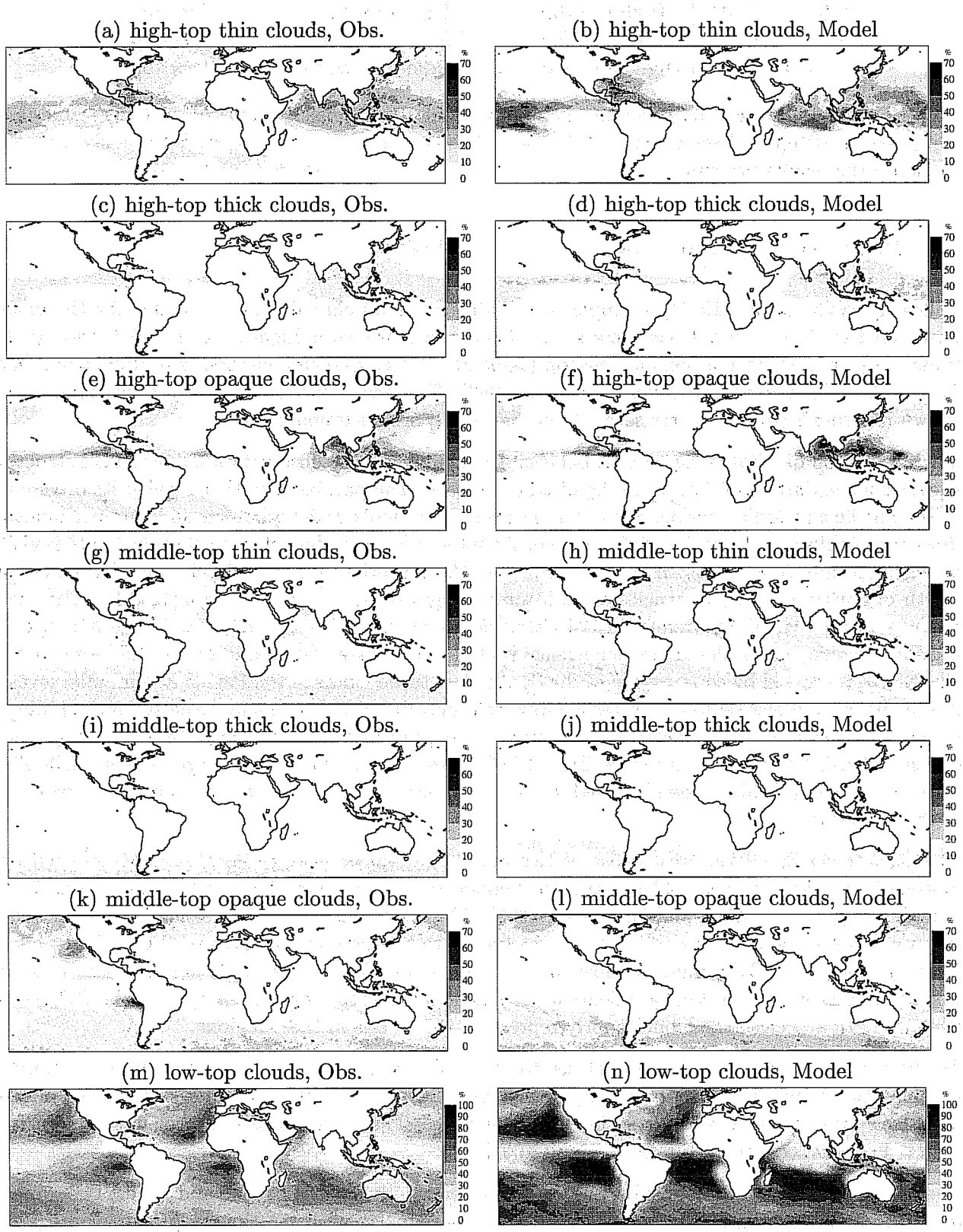

Figure 8: Occurrence frequency of high-, middle- and low-top clouds for the boreal summer season (JJA) over the oceans in the observations (left column) and in the model (right column).

	Ptop < 400 hPa	400 ≤ Ptop < 700 hPa	700 hPa ≤ Ptop
$0.05 \leq \tau < 0.7$	High-top thin	High-top thin	Low-top
$0.7 \leq \tau < 3.0$	High-top thick	Middle-top thick	Low-top
$3.0 \leq \tau$	High-top opaque	Middle-top opaque	Low-top

Table 2: Cloud classification based on nadir-equivalent 11 μm effective optical depth (τ) and cloud-top pressure (Ptop). Cases when $\tau < 0.05$ are classified as clear. This threshold was shown not to influence the results presented.

5.3 Retrieved cloud type

Following Wylie *et al.* (1994), a simple seven-category cloud classification is defined for the clouds, based on the CO_2-retrieved parameters, cloud top and emissivity: high-top thin, thick and opaque, middle-top thin, thick and opaque, low-top (table 2). The CO_2-slicing method is particularly reliable for the three high-cloud categories (Jin *et al.* 1996). The occurrence frequency of each cloud type is shown in figure 7 (boreal winter season) and figure 8 (boreal summer season).

There is a good qualitative agreement between the model and the observation for the ITCZ structure: the seasonal variations of the narrow-banded structure are comparable in both, as well as its broadening in the Pacific and Indian oceans due to large warm-ocean pools, Indonesian low and summer monsoon flows (e.g. Waliser and Gautier 1993). As seen from the infrared radiometer, most of the ITCZ is visible as high-top thin clouds, with smaller occurences of the two other high-top cloud types. In the portion North of Australia, the frequencies of high-top thin and opaque clouds are comparable. The model appears to produce higher frequencies of cirrus clouds in the ITCZ, in particular in the Atlantic and the East Pacific, where the model occurrence is about 50% instead of about 20% in the observations. The SPCZ is created by convergence of the South-East trade winds in the Pacific and mainly develops in the austral summer season. It is reasonably well reproduced by the model, even though middle-top thin clouds appear in the model in austral summer, and not in the observations. Similarly, the austral summer South Atlantic Convergence Zone (SACZ) and South Indian Convergence Zone (SICZ) as defined by Cook (2000) can be identified in the model, even if the cloud classification differs from that of the observation.

The stratus clouds off the west coast of the subtropical continents are usually associated with atmospheric subsidence over cold sea surface temperature with sharp temperature inversions in the boundary layer (e.g. Klein and Hartmann 1993). These regions are mainly cloud free in the model (Figure 5), even though the stratus clouds are known to be dense and numerous. Surprisingly, off the Peruvian coast and California, the observations report middle-top clouds. It is likely that temperature inversions and low vertical gradients induce higher cloud-tops than in reality with the CO_2-slicing technique. In any case, the model poorly represents the clouds in these regions.

As the westward trade winds come closer to the ITCZ, where the sea surface is warmer, cumulus becomes the dominant cloud type (e.g. Klein and Hartmann 1993). From the observed infrared radiances, large occurrences of low clouds are depicted. The occurrences of low clouds as seen from the model radiances are even higher (about 100%).

The storm tracks in both hemispheres have a high variability in both space and time. They appear in all three cloud categories in the observations. Consistently with the cloud-top histograms (figure 6), the model storm tracks have less high clouds. The model also appears to under-represent the transmissive clouds.

As a complementary study (not shown), the main tropical and extra-tropical cyclones have been individually examined. No systematic deficiency could be identified for the mid-latitude fronts, other

than the above-mentioned misrepresentation of high clouds, whereas Jakob and Rizzi (1997) described the fronts as too narrow in a previous version of the model. On the other hand, tropical cyclones appear to be too spread.

6 Discussion

In the previous sections cloudy radiances in two spectral regions and derived cloud information as observed by the TOVS instruments were compared with those simulated using short-range forecasts from the ECMWF model in the configuration used for the ERA-40 project. Apart from demonstrating the feasibility of such comparisons (see also Morcrette 1991a; Rizzi 1994; Shah and Rind 1995; Roca *et al.* 1997) a further aim of the study was to identify deficiencies in the representation of clouds in the ECMWF model, even though the use of the sole top-of-the-atmosphere radiation does not necessarily give a full insight into the characteristics of the model clouds. In summary of the previous sections the following features in the model have been identified.

- too little cloud-radiative effects of stratocumulus, apparent both at micro-wave and infrared wavelengths
- an underestimation of the frequency of very cold brightness temperatures in both tropics and mid-latitudes
- an overestimation of cloud top pressure (as derived by CO2-slicing) in mid-latitudes
- an overestimation of the frequency of occurrence of low clouds except in the stratocumulus regions
- on overestimation of the frequency of occurrence of high clouds in the ITCZ
- a strong underestimation of the frequency of clear sky situations, when they are defined with a simple threshold test

The poor representation of stratocumulus clouds and their radiative effects found here is consistent with previous findings by Jakob (1999), Chevallier and Morcrette (2000), and Duynkerke and Teixeira (2001). It should be noted that although the recent increase of the vertical resolution of the ECMWF model from 31 to 60 model levels has slightly improved the simulation of this cloud type (Teixeira, 1999), the model errors remain large. The correct simulation of stratocumulus by GCMs has been identified as a major problem area and work is underway not only at ECMWF to improve their representation.

Various interesting results about the simulation of high clouds have emerged. The long-wave radiative effects of high clouds seems to be underestimated, indicated by the lack of very low brightness temperatures in the model. This indicates that the model changes introduced after similar findings by Rizzi (1994), Jakob and Rizzi (1997) and Klein and Jakob (1999), such as the modifications to cloud ice settling introduced by Gregory et al. (2000), have not fully solved this problem. In contrast Chevallier and Morcrette (2000) have reported an underestimation of outgoing long-wave radiation (OLR) in comparison to Cloud and the Earth's Radiant Energy System (CERES) measurements once the model results are averaged over several weeks. The findings here provide some insight into the reasons for this apparent contradiction. High clouds when present produce too high brightness temperatures. However, their frequency of occurrence is overestimated by the model. Hence, the lack of radiative effect of high clouds apparent in instantaneous point to point comparisons (Figure 3) is

(a) Threshold based on cloud-cover

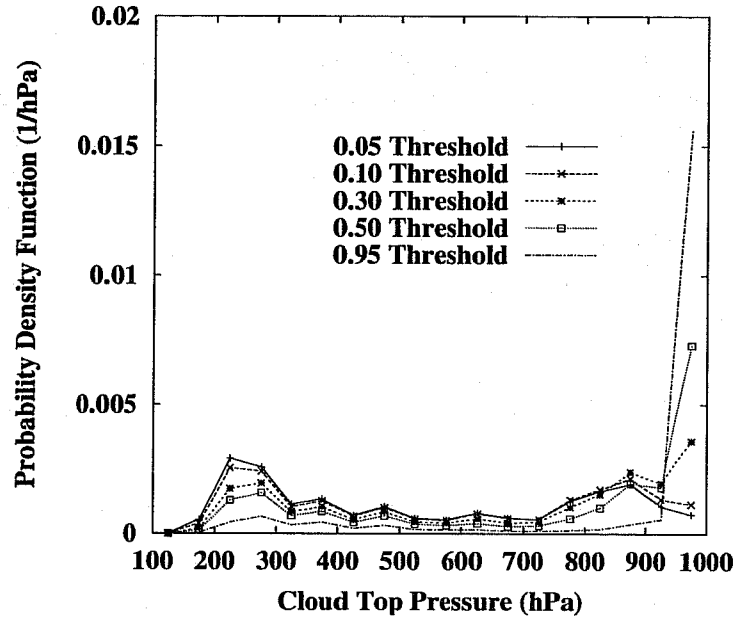

(b) Threshold based on ice water content (in kg/kg)

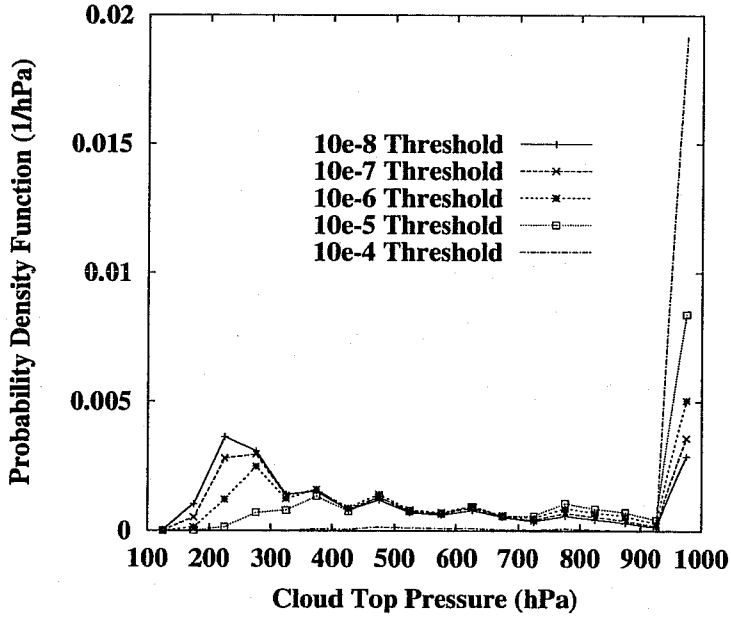

Figure 9: Histogram of model cloud-top pressure based on various thresholds. Starting from the top of the atmosphere, the cloud top is defined as the first level that reaches the corresponding threshold. Cloud-top pressures are set to 1000 hPa for clear-sky points. First 10 days of January 1987.

over-compensated by predicting their occurrence too frequently, leading to an overestimation of their long-wave effect in longer-term averages.

OLR and infrared brightness temperature are affected by many cloud parameters, such as cloud fraction, cloud condensate content, cloud top temperature, particle size and overlap. It is therefore difficult to assign the shortcomings in the radiative properties or derived quantities, such as cloud top pressure, to individual cloud parameters. An obvious way to further investigate which of the many cloud parameters is wrongly simulated by the model is to carry out sensitivity studies. However, this would require multiple integrations of the analysis system with various model versions for long periods of time, which is beyond the scope of this study. However, some insight might be gained by varying the assumptions of what is considered as a cloud in the model when estimating cloud top pressure. An example for this is shown in Figure 10. Here the model clouds are simply disregarded if their cloud fraction (top panel) or their cloud ice content (bottom panel) fall below a certain variable threshold (as indicated by the line style). The figure shows the variation of frequency distribution of cloud top pressure in the mid-latitudes when these thresholds are introduced. Note that the definitions of cloud top pressure in this figure are much simpler than in the CO_2-slicing method. In the top panel cloud top pressure is defined by finding the pressure of the first model level seen from the top with a cloud fraction larger than the threshold value. In the bottom panel cloud top pressure is defined the same way but using thresholds for cloud ice content instead of cloud fraction. It is evident that when defining cloud top pressure through cloud fraction the variation of the threshold value maintains a peak in the frequency distributions between 200 and 300 hPa. The situation is different for cloud ice content. Here using lower thresholds changes the shape of the distribution with the peak moving upwards. This indicates that the most likely cause of the overestimation of effective cloud top pressure in mid-latitudes as identified in Figure 6 is a lack of cloud ice or its radiative effects rather than an underestimation of cloud fraction. This finding is supported by the results of Klein and Jakob (1999) (their Figure 1).

Another problem identified is the apparent underestimation of the occurrence of clear sky situations in the model. Care has to be taken interpreting that result. It is evident in Figures 5, 7 and 8, that the largest regions with significant occurrence differences are those which usually exhibit low cloud covers such as the cumulus dominated trade wind regions. Typical values of cloud cover in both climatologies and model are on the order of 30 % and individual clouds are at most a few kilometres in horizontal extent. As the model resolution (about 60 km) is lower than the satellite one (about 20 km close to nadir), higher cloud frequencies are expected in the model.

As illustrated here, while not assimilated, cloudy-affected TOVS data are a key element of the monitoring of the ECMWF 40-year re-analysis. As a consequence, the model radiances and the CO_2-derived cloud variables from the model and from the HIRS observations will be part of the archive for the period following the first TOVS launch in 1978. The cloud variables derived from the observations will be a product of the re-analysis of direct climatological relevance. In addition they will help to validate the inter-annual variations of the model. The deficiencies identified here appear to be major challenges for modellers. Work is currently under way at ECMWF to remedy some of the problems highlighted here, in particular in the area of boundary-layer clouds.

Compositing and case studies (e.g., Klein and Jakob 1999) will be used to further refine the analysis of the model deficiencies in ERA-40 as well as in the operational analyses. Also, ongoing work is based on complementary satellite data such as SSM/I and geostationary imagery.

7 Prospects for the assimilation of cloudy radiances

7.1 Variational assimilation

In previous sections, the HIRS/2 and MSU data were shown to provide insight into the quality of the cloudiness simulated by the model. The diagnoses presented are expected to help improving the model parameterisations. Objective feedback may be obtained through data assimilation. However, as stated in the introduction, cloud analysis has been a challenge for global assimilation systems although in meso-scale models cloud analyses based on nudging techniques have been introduced (e.g. Lipton 1993; McPherson 1996; Bayler et al. 2000).

The present ECMWF assimilation scheme is a four-dimensional variational system (4D-Var) described by Courtier *et al.* (1994). The 4D-Var system seeks an optimal balance between observations and the dynamics of the atmosphere by finding a model trajectory $\mathbf{x}(t)$ which is as close as possible to the observations available during a given time period $[t_0, t_n]$. The model trajectory $\mathbf{x}(t)$ is completely defined by the initial state $\mathbf{x_0}$ at time t_0. The misfit to observations $\mathbf{y}$ and to background (or first-guess) model state $\mathbf{x}^b$ is measured by an objective cost-function, that is being minimised during the assimilation process.

As described by Marécal and Mahfouf (2000) and by Chevallier and Mahfouf (2001), one-dimensional variational assimilation (1D-Var) systems is suitable for such studies. The principle of the 1D-Var is similar to that of 4D-Var, but the control vector $\mathbf{x}$ represents only a single column and the time dimension is not included. The cost-function reduces to:

$$J(\mathbf{x}) = \frac{1}{2}(\mathbf{x}-\mathbf{x}^b)^T\mathbf{B}^{-1}(\mathbf{x}-\mathbf{x}^b) + \frac{1}{2}(H(\mathbf{x})-\mathbf{y})^T\mathbf{R}^{-1}(H(\mathbf{x})-\mathbf{y}) \quad (4)$$

where $\mathbf{y}$ is the vector of observations, H is the operator simulating the observed data from the model variable $\mathbf{x}$, $\mathbf{R}$ is the observation error covariance matrix (measurement errors and representativeness errors, including errors in H), and $\mathbf{B}$ is the background error covariance matrix of the state $\mathbf{x}^b$. Superscripts -1 and T denote respectively inverse and transpose matrix.

The present study makes use of the 1D-Var code described by Marécal and Mahfouf (2000), Fillion and Mahfouf (2000) and Chevallier and Mahfouf (2001). The minimiser is a limited memory quasi-Newton method, the M1QN3 software developed at Institut National de Recherche en Informatique et en Automatique (INRIA) (Gilbert and Lemaréchal, 1989).

7.2 1D-Var experiment

In order to test a variational assimilation of cloudy radiances, a set of 20 atmospheric profiles is extracted from the ECMWF 6-hour forecast archives. For each of them, a 1D-Var assimilation is performed.

The 1D-Var control variables consist of profiles of temperature, water vapour, ozone, cloud cover, liquid and ice water contents from the top of the atmosphere to the surface (60 levels) in addition to the surface temperature (a total of 361 elements).

Synthetic brightness temperature observations of HIRS/3 channels 4 to 8 (similar to HIRS/2 channels 4 to 8) and AMSU channels 1 ($23.8GHz$) and 2 ($31.4GHz$) are computed with the cloudy radiative transfer model. HIRS/3 and AMSU respectively replace the HIRS/2 and MSU instruments on the NOAA satellites since NOAA-15. Together they form the Advanced TOVS (ATOVS) instrument. In the 1D-Var, the brightness temperatures are simulated with RTTOV, taking the cloud profile into

account. A simple observation error covariance matrix $\mathbf{R}$ is used: The standard deviation is set to 1 K in each channel, with no correlation between the channels.

These experiments aim at testing the capacity of the 1D-Var to retrieve cloud profiles when there is no cloud in the background. Therefore, the 1D-Var background $\mathbf{x}^b$ is defined as the profiles of temperature, water vapour and ozone of the archived situation, but cloud cover, liquid and ice water contents are set to ϵ. ϵ is a very small value (10^{-4} for cloud cover and 10^{-10} kg/kg for cloud condensate), that allows for non-zero derivatives of the cloud variables at the first step of the 1D-Var. For temperature, water vapour, and ozone, the background error covariance matrix $\mathbf{B}$ is specified according to the operational 4D-Var for unbalanced quantities. For cloud variables, vertical correlations are defined with a gaussian shape of standard deviation 100 hPa. The specified standard deviations are large in the troposphere: 1.0 for cloud cover, 10^{-3} for liquid water and 10^{-5} for ice water. The factor 100 between liquid and ice water was chosen because of the much smaller sensitivity of the radiances to liquid water. For temperatures below 260 K (respectively above 274 K), the liquid (respectively ice) water standard deviations are set to zero. The specified standard deviations are also set to zero above the tropopause, for both liquid and ice water.

Two 1D-Var experiments are illustrated in Figures 10 and 11. They are extracted respectively from a front in the Northern Atlantic and from the Atlantic part of the ITCZ. In both cases, the temperature, water vapour, and ozone increments are negligible. The retrieved cloud cover profile has a double-peak structure. The highest peak corresponds to ice water and the lowest one to liquid water. The retrieved condensate profiles have a gaussian shape, consistently with the specified error covariance matrix, but the width is significantly larger than the specified one.

The retrieved shapes of the cloud profiles do not accurately reproduce the "truth" (i.e. the synthetic observations). In particular, the retrieved cloud cover is underestimated close to the surface. However, the retrieved shapes appear to be physically reasonable. Moreover, the brightness temperatures of the 1D-Var output fit the observed ones to within 0.5 K for the infrared channels (background departures were more than 10 K for the lowest channels) and to within 2.0 K for the microwave ones (background departures were about 4 K). Similarly, the 1D-Var can suppress cloudiness when there is some in the background and none in the observation (not shown). An intermediate case is shown in Figure 12, where the 1D-Var modifies an existing cloudiness profile when the cloud is also present in the observation.

On a few cases among those tested the 1D-Var does not perform well. They correspond to low-cloud situations (not shown). The minimisation produces high ice cloud profiles together with unrealistic temperature, water vapour, and ozone increments. Similarly, even when there is no cloud both in the background and in the observations, ice cloud increments can be produced.

7.3 Single-column model experiment

As seen in the previous section, the ATOVS radiances in the 1D-Var framework may be used to create or suppress profiles of cloudiness. The ability of the model to retain information from cloud initial conditions is studied with the ECMWF single-column model. Use is made of case 2 from the GEWEX Cloud System Study (GCSS) working group 4. As described by Krueger and Lazarus (1999), this case is a situation of deep convection over five days based on the Tropical Oceans Global Atmosphere (TOGA) Coupled Ocean-Atmosphere Response Experiment (COARE). The time evolution of the lateral boundaries of the column is prescribed.

Figure 13b shows the time evolution of the cloud cover over the five days in the control run. In the experiment run (Figure 13a), cloudiness is suppressed every 12 hours, as if a satellite instrument provided the information that no cloud is present in reality. The suppression of the cloud is simply

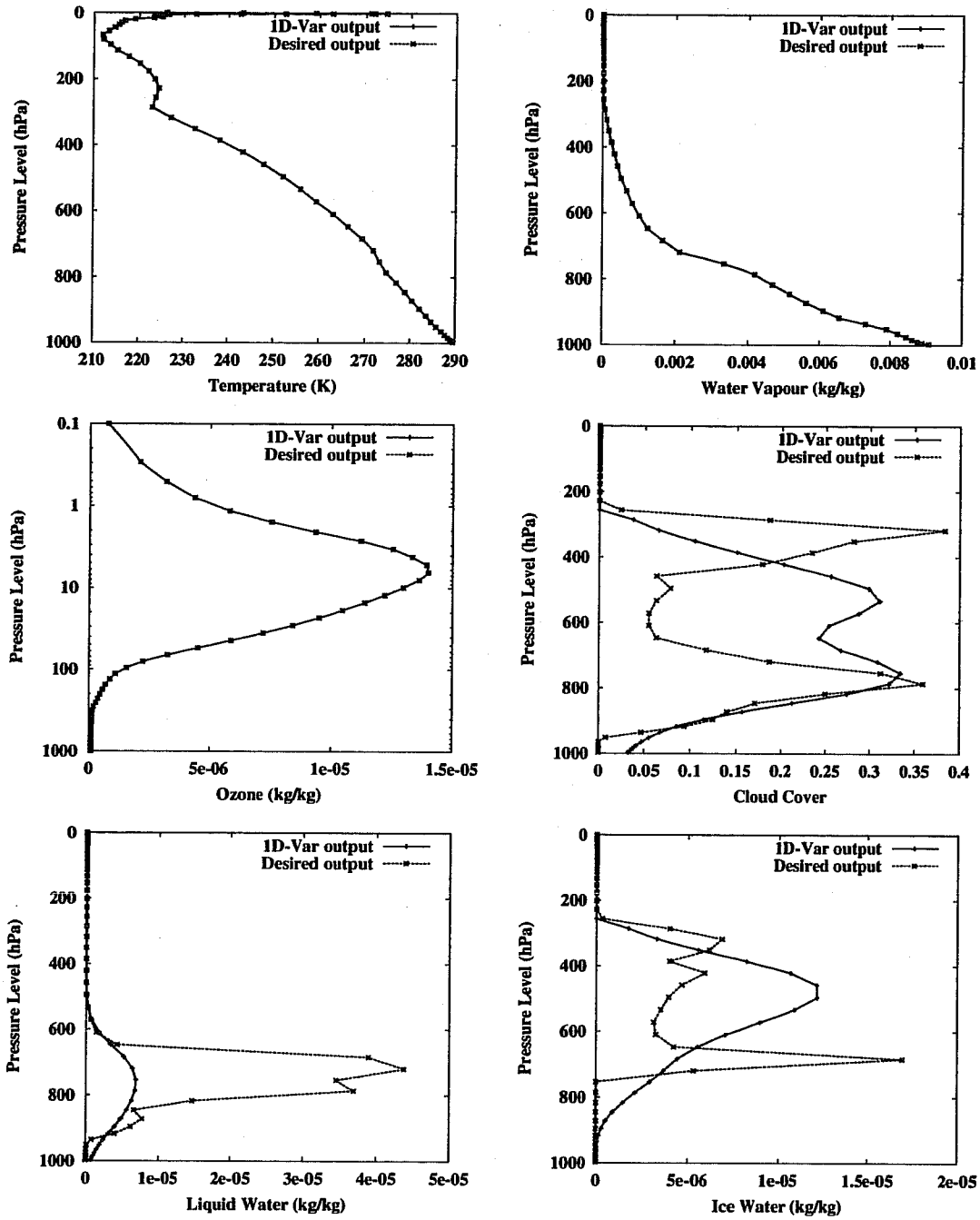

Figure 10: 1D-Var output and desired output profiles. Case from a Northern Atlantic front. The background profiles does not have any cloudiness.

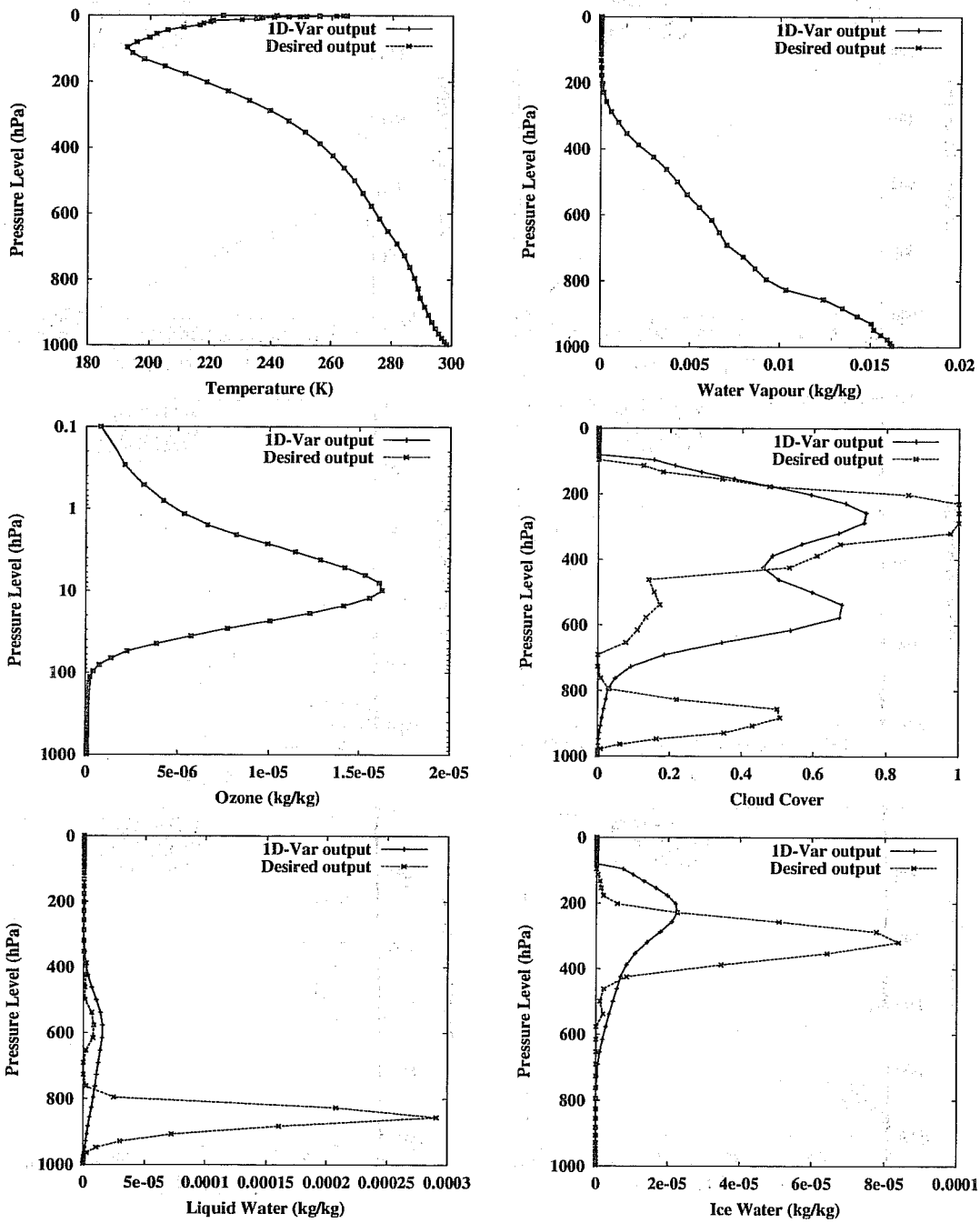

Figure 11: Same as previous but for a deep convection case.

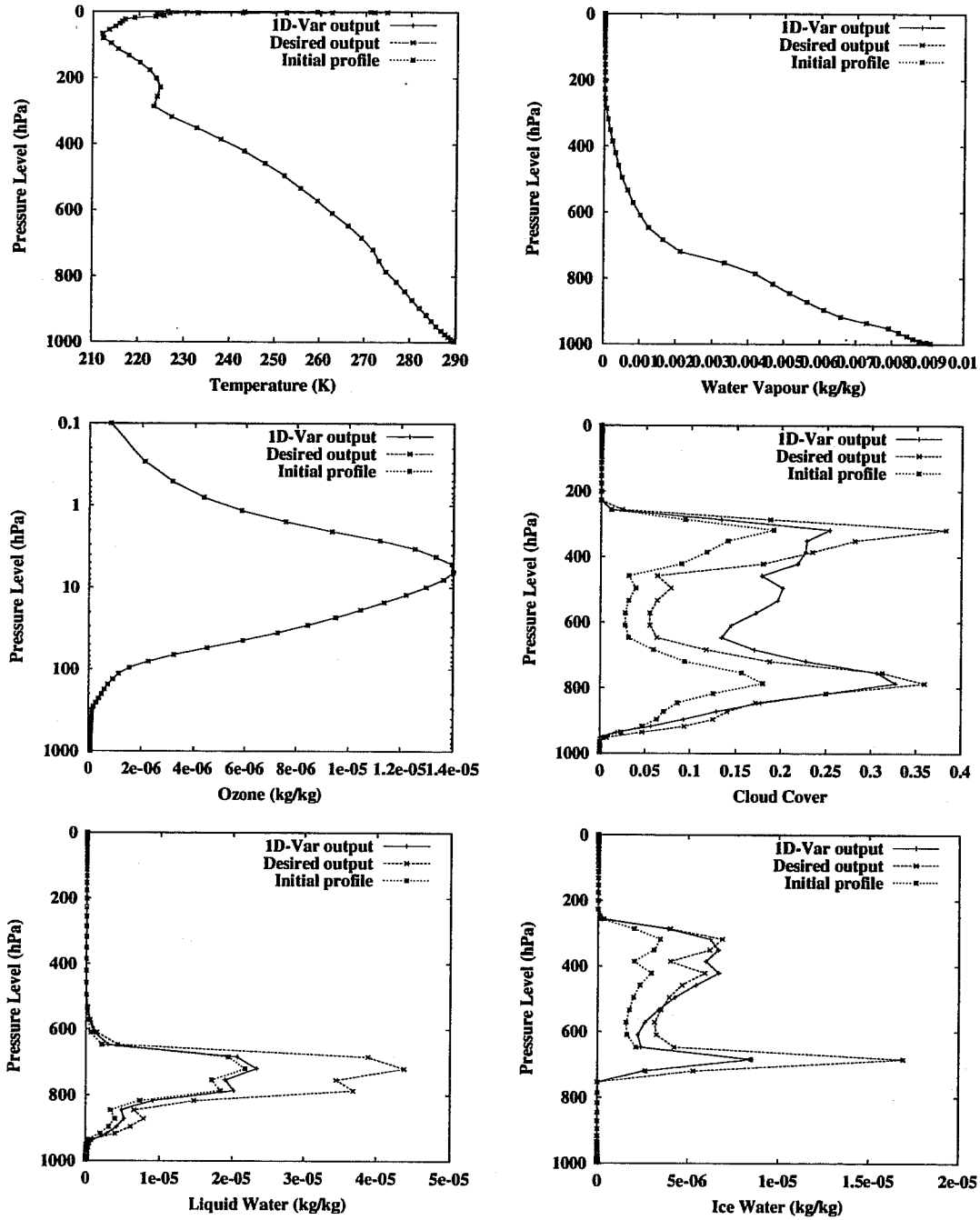

Figure 12: Background, 1D-Var output and desired output profiles. Case from a Northern Atlantic front. The values of the background profile of cloud cover, liquid and ice water are half those of the observed profile (desired output).

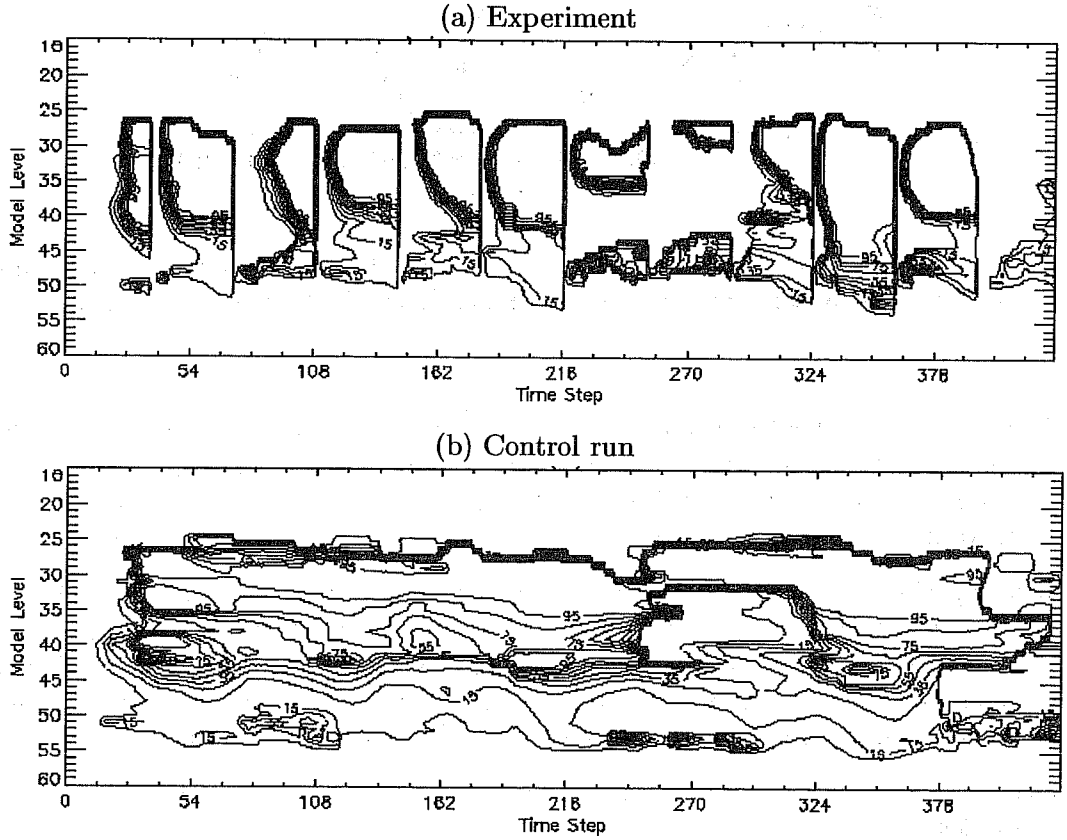

Figure 13: Time series of simulated cloud cover. The time step is 20 minutes. Single-column model simulations of a case of tropical deep convection. In the experiment (top), the cloud cover and condensate are set to 0.0 and the relative humidity to 0.6 every 12 hours.

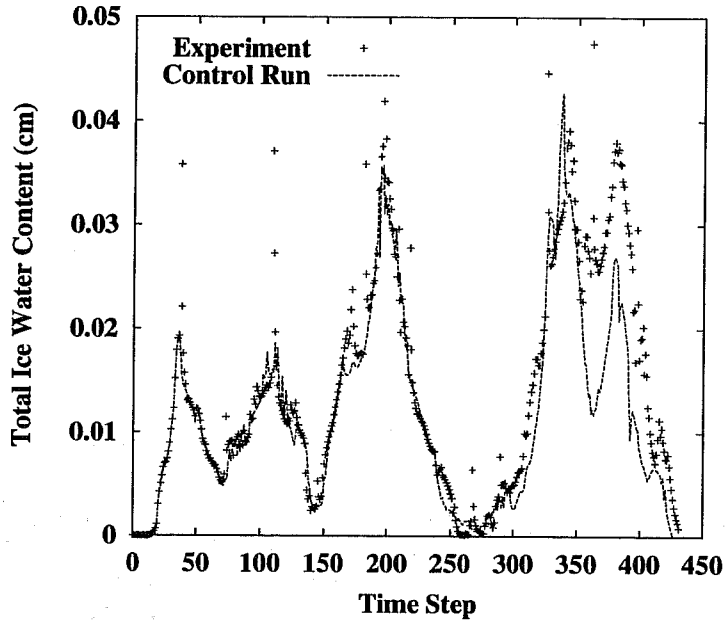

Figure 14: Time series of total ice water content. The time step is 20 minutes. One-column model simulations of a case of tropical convection. In the experiment, the total ice water content is doubled every 12 hours.

performed by setting the cloud variables (cloud cover and condensate) to 0 and by modifying the humidity so that the relative humidity equals 60%. The "analysis" times appear clearly in Figure 13a. Indeed the cloudiness forms again after about one hour. The large-scale forcing is sufficient to recreate clouds quickly, while no additional depletion process is introduced between two "analysis" times.

An additional experiment is presented. Every 12 hours, the ice content is doubled at each model level. Figure 14 shows the time series of the total ice water content both in the control and in the experiment run. The ice introduced is shown to fall out after a couple of time steps. Indeed the fall speed of the ice particles is proportional to the ice content in the model parametrisation (Heymsfield and Donner 1990). Also no additional source of ice is introduced between two "analysis" times.

This simple experiment emphasises the need of modifications to the model dynamics consistently with the cloud variables.

7.4 Discussion

The present study shows that information about liquid and ice water that is contained in the ATOVS radiances can be extracted by a 1D-Var scheme. In non-rainy areas, clouds can be suppressed, created or modified to fit the observed radiances. In rainy areas, microwave radiances are significantly affected but no rain absorption/scattering parametrisation has been introduced yet in the radiation model. This will be further studied.

Because the vertical resolution of cloud information in radiances is limited, the increments strongly rely on the specified background error covariances. In terms of physical values, the retrieved cloudiness may not be more accurate than a cloud retrieval not using model cloudiness, like the CO_2-slicing method. As illustrated by Jin *et al.* (1996), the latter methods also suffer from various limitations. The advantage of producing cloud increments in a variational framework is the possibility of also having consistent atmospheric variables, like temperature and wind. This is essential for forecast

models, since the single-column model experiment shows that a dynamics that is inconsistent with the cloud profiles loses the analysed cloud information within a few model time steps. The consistency can be achieved either with proper coupling in the background error matrix, or by relating the cloud increments to the dynamical variables. The latter issue is being investigated (Janisková *et al.* 2000). As the specification of the error background matrix is crucial for the result of the variational analysis, its formulation in the ECMWF system is also being revised, in particular for water vapour. Additional information, like that one provided by visible channels, may also be used to make the error matrix dependent on the local dynamics.

With new instruments dedicated to the observation clouds, like CloudSat (NASA) or the Earth CARE (ESA), the situation is likely to evolve from the present situation discussed in this paper. In particular, the use of active instruments (radar and lidar) should improve the vertical resolution and provide more direct cloud property information, such as ice water content or particle size.

Acknowledgements

D. P. Wylie and P. Menzel provided the initial version of the CO_2-slicing subroutine. The authors are grateful to J.-J. Morcrette and to M. Janisková for fruitful discussions about the issues raised in this paper. The help of Erik Andersson and S. Saarinen in introducing the full-sky radiance computation in the ECMWF forecast system was greatly appreciated. The INRIA (Institut National de Recherche en Informatique et Automatique) provided the M1QN3 minimisation code. This work was done partly at the Satellite Application Facility on Numerical Weather prediction which is co-sponsored by Eumetsat. A. Simmons helped to improve the initial manuscript.

References

Andersson, E., J. Haseler, P. Undén, P. Courtier, G. Kelly, D. Vasiljevic, C. Branković , C. Cardinali, C. Gaffard, A. Hollingsworth, C. Jakob, P. Janssen, E. Klinker, A. Lanzinger, M. Miller, F. Rabier, A. Simmons, B. Strauss, J.-N. Thépaut, and P. Viterbo, 1998: The ECMWF implementation of three-dimensional variational assimilation (3D-Var). III: Experimental results. *Q. J. Roy. Meteor. Soc.*, **124**, 1831-1860.

Bayler, G. M., R. M. Aune, and W. H. Raymond, 2000: NWP initialization using GOES sounder data and improved modeling of non-precipitating clouds. *Mon. Wea. Rev.*, **128**, 3911-3920.

Chevallier, F., and J.-J. Morcrette, 2000: Comparison of model fluxes with surface and top-of-the-atmosphere observations. *Mon. Wea. Rev.*, **128**, 3839-3852.

Chevallier, F., and J.-F. Mahfouf, 2001: Evaluation of the Jacobians of infrared radiation models for variational data assimilation. *J. Appl. Meteor.*, **40**, 1445-1461.

Cook, K. H., 2000: The South Indian Convergance Zone and interannual rainfall variability over Southern Africa. *J. Climate*, **13**, 3789-3804.

Courtier, P., J.-N. Thépaut, and A. Hollingsworth, 1994: A strategy, for operational implementation

of 4D-Var, using an incremental approach. *Q. J. Roy. Meteor. Soc.*, **120**, 1367-1388.

Courtier, P., E. Andersson, W. Heckley, J. Pailleux, D. Vasiljević, M. Hamrud, A. Hollingsworth, F. Rabier, and M. Fisher, 1998: The ECMWF implementation of three dimensional variational assimilation (3D-Var). Part I.: formulation. *Q. J. Roy. Meteor. Soc.*, **124**, 1783-1808.

Duynkerke, P. G., and J. Teixeira, 2001: A comparison of the ECMWF re-analysis with FIRE I obsevrations: diurnal variation of marine stratocumulus. *J. Clim.*, **14**, 1466-1478.

Ebert, E. E. and J. A. Curry, 1992 : A parameterization of cirrus cloud optical properties for climate models. *J. Geophys. Res.*, **97D**, 3831-3836.

Eyre, J. R., 1991: A fast radiative transfer model for satellite sounding systems. *ECMWF Technical Memorandum No. 176*, 28 pp.

Fillion, L., and J.-F. Mahfouf, 2000: Coupling of moist-convective and stratiform precipitation processes for variational data assimilation. *Mon. Wea. Rev.*, **128**, 109-124.

Fouquart, Y. and B. Bonnel, 1980: Computation of solar heating of the Earth's atmosphere: a new parameterization. *Beitr. Phys. Atmosph.*, **53**, 35-62.

Gilbert, J. C., and C. Lemaréchal, 1989: Some numerical experiments with variable-storage quasi-Newton algorithms. *Mathematical Programming*, **45**, 407-435.

Gregory, D., J.-J. Morcrette, C. Jakob, A. C. M. Beljaars, and T. Stockdale, 2000: Revision of convection, radiation and cloud schemes in the ECMWF Integrated Forecasting System. *Q. J. Roy. Meteor. Soc.*, **126**, 1685-1710.

Harris, B. A., and G. Kelly, 2001: A Satellite Radiance Bias Correction Scheme for Radiance Assimiliation. *Q. J. Roy. Meteor. Soc.*, **127**, 1453-1468.

Heymsfield, A. J. and L. J. Donner, 1990: A scheme for parametrizing ice-cloud water content in general circulation models. *J. Atmos. Sci.*, **47**, 1865-1877.

Hortal, M., 1999: The development and testing of a new two-time-level semi-Lagrangian scheme (SETTLS) in the ECMWF forecast model. ECMWF Technical Memorandum No. 292, 17 pp. [available from ECMWF, Shinfield Park, Reading, Berks. RG2 9AX, UK].

Hufford, G., 1991: A model for the complex permittivity of ice. *Int. J. Infrared Millimeter Waves*, **12**, 677-681.

Jakob, C., 1999: Cloud cover in the ECMWF reanalysis. *J. Climate*, **12**, 947-959.

Jakob, C., 2000: The representation of cloud cover in atmospheric general circulation models. *PhD thesis*, Ludwig-Maximilians-Universität München, 193 pp.

Jakob, C., and R. Rizzi, 1997: Evaluation of model OLR in cloudy regions using TOVS-1B data. *Proc. of the Int. TOVS Study Conference, Igls, Austria, 20-26 February 1997*, 197-206.

Jakob, C., and S. A. Klein, 2000: A parametrization of the effects of cloud and precipitation overlap for use in general-circulation models. *Q. J. Roy. Meteor. Soc.*, **126**, 2525-2544.

Jakob, C., E. Andersson, A. Beljaars, R. Buizza, M. Fisher, E. Gérard, A. Ghelli, P. Janssen, G. Kelly, A. P. McNally, M. Miller, A. Simmons, J. Teixeira, and P. Viterbo, 2000: The IFS cycle CY21r4 made operational in October 1999. *ECMWF Newsletter*, **87**, 2-9.

Janisková, M., J.-F. Mahfouf, F. Chevallier, and J.-J. Morcrette, 2000: Linearized physics for the assimilation of cloud properties. *ECMWF/ EuroTRMM Workshop on Assimilation of Clouds and Precipitation, Reading, UK, 6-9 November 2000.*

Jin, Y, W. B. Rossow, and D. P. Wylie, 1996: Comparison of the climatologies of high-level clouds from HIRS and ISCCP. *J. Climate*, **9**, 2850-2879.

Klein, S. A., and D. L. Hartmann, 1993: The seasonal cycle of low stratiform clouds. *J. Climate*, **6**, 1587-1606.

Klein, S. A., and C. Jakob, 1999: Validation and sensitivities of frontal clouds simulated by the ECMWF model. *Mon. Wea. Rev.*, **127**, 2514-2531.

Kidwell, K. B., 1998: NOAA polar orbiter user's guide. Technical report, U. S. Dept of Commerce/ NOAA/ NESDIS.

Krueger, S. K., and S. M. Lazarus, 1999: Intercomparison of multi-day simulations of convection during TOGA COARE with several cloud-resolving and single-column models. *Preprints, 23rd Conference on Hurricanes and Tropical Meteorology, Dallas, TX, Amer. Meteor. Soc.*, 643-647.

Liebe, H. J., T. Manabe, and G. A. Hufford, 1989: Millimeter wave attenuation and delay rates due to fog/ cloud conditions. *IEEE Trans. Antennas Propag.*, **37**, 1617-1623.

Lipton, A. E., 1993: Cloud shading retrieval and assimilation in a satellite-model coupled mesoscale analysis system. *Mon. Wea. Rev.*, **115**, 3062-3080.

Marécal, V., and J.-F. Mahfouf, 2000: Variational retrieval of temperature and humidity profiles from TRMM precipitation data. *Mon. Wea. Rev.*, **128**, 3853-3866.

Masuda, K., T. Takashima, and Y. Takayama, 1988: Emissivity of Pure and Sea Waters for the Model

Sea Surface in the Infrared Window Regions. *Remote Sensing of the Environment*, **24**, 313-329.

McNally, A. P., 2000: The occurence of cloud in meteorologically sensitive areas and the implications for infrared sounders. Proc. of the *Int. TOVS Study Conference, Budapest, Hungary, 20-26 September 2000.*

McPherson, B., B. J. Wright, W. H. Hand and A. J. Maycock (1996): The impact of MOPS moisture data in the UK Meteorological Office mesoscale data assimilation scheme *Mon. Wea. Rev.*, **124**, 1746-1766.

Menzel, W. P., D. P. Wylie, and K. I. Strabala, 1992: Seasonal and diurnal changes in cirrus clouds as seen in four years of observations with the VAS. *J. Appl. Meteor.*, **31**, 370-385.

Mlawer, E. J., S. J. Taubman, P. D. Brown, M. J. Iacono, and S. A. Clough, 1997: Radiative transfer for inhomogeneous atmospheres : RRTM, a validated correlated-k model for the longwave. *J. Geophys. Res.*, **102**, 16663-16682.

Morcrette, J.-J., 1991a: Evaluation of model-generated cloudiness: satellite observed and model-generated diurnal variability and brightness temperature. *Mon. Wea. Rev.*, **119**, 1205-1224.

Morcrette, J.-J., 1991b: Radiation and Cloud Radiative Properties in the European Centre for Medium Range Weather Forecasts forecasting system. *J. Geophys. Res.*, **96:D5**, 9121-9132.

Morcrette, J.-J., and C. Jakob, 2000: The response of the ECMWF model to changes in cloud overlap assumption. *Mon. Wea. Rev.*, **128**, 1707-1732.

Ou, S.-C., and K.-N. Liou, 1995: Ice microphysics and climatic temperature feedback. *Atmos. Res.*, **35**, 127-138.

Price, J.C., 1991: Timing of NOAA afternoon passes. *Int. J. Remote Sensing*, **12**, 193-198.

Prigent, C., W. B. Rossow, and E. Matthews, 1997: Microwave land surface emissivities estimated from SSM/I observations. *J. Geophys. Res.*, **102:18**, 21867-21890.

Rabier, F., A. McNally, E. Andersson, P. Courtier, P. Unden, J. Eyre, A. Hollingsworth and F. Bouttier, 1998 : The ECMWF implementation of three dimensional variational assimilation (3D-Var). Part II : Structure functions. *Q. J. Roy. Meteor. Soc.*, **124**, 1809-1829.

Räisänen, P., 1998: Effective longwave cloud fraction and maximum-random overlap clouds - a problem and a solution. *Mon. Wea. Rev.*, **126**, 3336-3340.

Rizzi, 1994: Raw HIRS/2 radiances and model simulations in the presence of clouds. ECMWF Technical Memorandum No. 73, 29 pp.

Roca, R., L. Picon, M. Desbois, H. Le Treut, and J.-J. Morcrette, 1997: Direct comparison of Meteosat water vapor channel data and general circulation model results. *Geophys. Res. Letters*, **24**, 147-150.

Saunders, R., M. Matricardi, and P. Brunel, 1999: An improved fast radiative transfer model for assimilation of satellite radiance observations. *Quart. J. Roy. Meteor. Soc.*, **125**, 1407-1425.

Shah, K. P., and D. Rind, 1995: Use of microwave brightness temperatures with a general circulation model. *J. Geophys. Res.*, **100:D7**, 13,841-13,874.

Simmons, A. J., and J. K. Gibson (Eds), 2000: The ERA-40 project plan. *ERA-40 Project Report Series No. 1*, 62 pp.

Smith, W. L. and C. M. R. Platt, 1978: Intercomparison of radiosonde, ground-based laser, and satellite-deduced cloud heights. *J. Appl. Meteor.*, **17**, 1796-1802.

Smith, E. A., and L. Shi, 1992: Surface forcing of the infrared cooling profile over the Tibetan plateau. Part I: Influence of relative longwave radiative heating at high altitude. *J. Atmos. Sci.*, **49**, 805-822.

Teixeira, J., 1999: The impact of increased boundary layer resolution on the ECMWF forecast system. *ECMWF Technical Memorandum*, **268**, 55 pp. [available from ECMWF, Shinfield Park, Reading, Berks. RG2 9AX, UK]

Tiedtke, M., 1993: Representation of clouds in large-scale models. *Mon. Wea. rev.*, **121**, 3040-3061.

Ulaby, F. T., R. K. Moore, A. K. Fung, 1981: Microwave remote sensing: active and passive. Volume I. Artech House, 456 pp.

Van den Hurk, B. J. J. M., P. Viterbo, A. C. M. Beljaars, and A. K. Betts, 2000: Offline validation of the ERA40 surface scheme. ECMWF Technical Memorandum No. 295, 42 pp. [available from ECMWF, Shinfield Park, Reading, Berks. RG2 9AX, UK].

Waliser and Gautier, 1993: A satellite-derived climatology of the ITCZ. *J. Climate*, **6**, 2162-2174.

Washington, W. M. and D. L. Williamson, 1977: A description of the NCAR GCM. In *Methods in Computational Physics*, **17** J. Chang. (Ed.), Academic Press, New York, 111-172.

Wylie, D. P., W. P. Menzel, H. M. Woolf, and K. I. Strabala, 1994: Four years of global cirrus cloud statistics using HIRS. *J. Climate*, **7**, 1972-1986.

Wylie, D. P., and W. P. Menzel, 1999: Eight years of high cloud statistics using HIRS. *J. Climate*, **12**, 170-184.